

Generalized routhian calculations within the Skyrme–Hartree–Fock approximation

D. Samsøen, P. Quentin

Centre d'Etudes Nuclaires de Bordeaux-Gradignan (IN2P3-CNRS and Univ. Bordeaux-I), Gradignan, France

J. Bartel

Institut de Recherches Subatomiques (IN2P3-CNRS and Univ. Louis Pasteur), Strasbourg, France

Abstract

We consider here variational solutions in the Hartree–Fock approximation upon breaking time reversal and axial symmetries. When decomposed on axial harmonic oscillator functions, the corresponding single particle triaxial eigenstates as functions of the usual cylindrical coordinates (r, θ, z) are evaluated on a mesh in r and z to be integrated within Gauss–Hermite and Gauss–Laguerre approaches and as Fourier decompositions in the angular variable θ . Using an effective interaction of the Skyrme type, the Hartree–Fock hamiltonian is also obtained as a Fourier series allowing a two dimensional calculation of its matrix elements. This particular choice is shown to lead in most cases to shorter computation times compared to the usual decomposition on triaxial harmonic oscillator states. We apply this method to the case of the semi-quantal approach of large amplitude collective motion corresponding to a generalized routhian formalism and present results in the $A = 150$ superdeformed region for the coupling of global rotation and intrinsic vortical modes in what is known after Chandrasekhar as the S -ellipsoid coupling case.

1 Introduction

In microscopic calculations within the Hartree–Fock approximation, one-body eigenstates wave functions can be either evaluated numerically on a mesh or decomposed on some truncated set of orthogonal functions. In the former case, it is necessary to solve the static Schrödinger-like integro-differential or in the Skyrme case partial-derivative equations which can prove to be a long process, whereas in the latter, one has to compute matrix elements of the Hartree–Fock hamiltonian on the set and then diagonalize the obtained matrix. This

second method is known to be rather efficient in terms of computation time. However, as one is bound to use only a truncated basis, the obtained results are dependent on the basis parameters and size. Nevertheless the energy difference between the truncated solution and the exact one (which would correspond to an infinite basis and can be approached by the former method) may in some cases be evaluated (see e.g. [1]).

In order to describe a compact system of particles interacting through mostly attractive two body forces, one often chooses as a basis set, eigenfunctions of a deformed harmonic oscillator single particle hamiltonian. One truncates it for instance [1] by only retaining the eigenstates whose eigenenergies are lower than some truncation energy reference. The obtained solutions thus depend on both the truncation energy and the deformation parameters of the harmonic oscillator basis. For a given truncation, the deformation parameters to be used are obtained by a minimization of the energy with respect to these parameters. When describing axially symmetric nuclei, it is appropriate to use axially symmetric harmonic oscillator wave functions, all the calculations being then performed in two dimensions. To the best of our knowledge, when projecting triaxially shaped solutions on a single particle basis, only triaxial harmonic oscillator wave functions have been used [2–4]. We present here an alternative way to describe triaxial shapes by using an axially symmetrical basis. Axially symmetric wave functions are eigenstates of the projection of the angular momentum on the quantization axis. By mixing states with different eigenvalues for this operator, one can obtain triaxial wave functions. As a matter of fact, in the position representation, those functions are expressed for any point of the (r, z) plane as a complex Fourier series in the angular variable θ .

Using, as we will do here, an effective interaction of the Skyrme type (namely in the SkM* parametrisation [5]), the total energy of the nucleus is obtained by integrating an energy density functional which, as well as the potentials of the Hartree–Fock hamiltonian, is expressed in terms of sums, products and integer and non-integer powers of some local densities. With our choice of axially symmetric basis states as we will show, those densities, and hence the Hartree–Fock potentials and energy functional, are obtained as real Fourier series in the angular variable. By integrating the energy functional over the whole space, only the first term of the Fourier series (which remains constant as a function of θ) is non vanishing. This component is calculated for each point in the (r, z) plane and then integrated in two dimensions. Using selection rules, the calculation of the Hartree–Fock hamiltonian matrix elements can also be performed through a single two-dimensional integral whereas when using triaxial wave functions, all these integrations would be three-dimensional. Our alternative method thus is expected to lead to shorter computation times provided that the number of axially symmetric basis wavefunctions necessary for an accurate description of the triaxial solution is not too large.

Even for triaxial shapes, high order Fourier components are exactly zero and the number of non vanishing components is determined by the truncation parameter. In practical cases, one can impose a cutoff in the maximal order of the retained components, due to the observed fast convergence of the numerical results with respect to this maximal order. For axially symmetric nuclei, only the first component of the densities are non vanishing. We are thus able to describe both axially symmetric and triaxial shapes within the same code by simply adjusting the maximal order of the Fourier decompositions. For largely triaxial shapes we can expect relatively important truncations effects within our method, which will lead to a reduced competitiveness of our approach with respect to those using triaxial basis.

This calculation method has been applied to physical situations of triaxial shapes combined with time-reversal symmetry breaking as obtained within the well known cranking (or routhian) approximation or within approaches corresponding to a generalization of the latter. This generalization which will be called below the generalized routhian formalism has been briefly sketched in a previous paper [6] and will be presented in more details in Ref. [7]. It allows us to describe the dynamics of a class of collective modes defined by a velocity field in a semi-quantal approach à la WKB. It reduces to the addition of a time-odd constraint $-\boldsymbol{\beta} \cdot \mathbf{p}$ to the static hamiltonian, where $\boldsymbol{\beta}$ is the classical collective velocity field under study and \mathbf{p} is the single particle momentum operator. The possible choices for the $\boldsymbol{\beta}$ -fields have been restricted by imposing the routhian eigenstates to be also eigenstates of the parity and of the signature operator with respect to the first axis.

This paper will be organized as follows. In Section 2 we will present our formalism with some calculation and computation details. Section 3 will be devoted to discussions about truncation effects and the computation time we expect to gain and will end with the comparison of our results with the literature. We will then turn to the generalized routhian formalism in the S -type ellipsoid case and present some preliminary results in section 4 before concluding and presenting perspectives of future work in section 5.

2 Hartree–Fock–Skyrme generalized routhian

2.1 One and N -body routhians

Within classical mechanics, the canonical form of the equations of motion is conserved under a canonical transformation of the dynamical variables by adding to the hamiltonian the time derivative of a generating function. In the case of a local transformation (i.e. involving only the coordinates), this time

derivative writes as

$$\frac{\partial G}{\partial t} = -\boldsymbol{\beta} \cdot \mathbf{p}, \quad (1)$$

where $\boldsymbol{\beta}$ is the collective velocity related to the transformation. In the quantum mechanical case, it can be shown [7] using a certain class of unitary transformations that the density matrix solution of the Hartree–Fock equation involving the generalized routhian

$$R = H - \frac{1}{2}(\boldsymbol{\beta} \cdot \mathbf{p} + \mathbf{p} \cdot \boldsymbol{\beta}) \equiv H - \boldsymbol{\beta} \cdot \mathbf{p} + \frac{i\hbar}{2}\text{div}\boldsymbol{\beta}. \quad (2)$$

in lieu of the hamiltonian H exhibits in the laboratory frame a dynamical content which corresponds to the collective velocity field $\boldsymbol{\beta}$. When spin degrees of freedom are present, it is necessary to also consider the spin-rotation collective mode. Considering a vortical velocity field, the routhian then writes

$$R = H - \boldsymbol{\beta} \cdot \mathbf{p} - \frac{\hbar}{2}\boldsymbol{\Omega} \cdot \boldsymbol{\sigma}, \quad (3)$$

where $\boldsymbol{\sigma}$ is the vector whose components are the three Pauli matrices. As an example, in the case of global rotation where the collective field is

$$\boldsymbol{\beta}_{\text{rot}} = \boldsymbol{\Omega} \times \mathbf{r}, \quad (4)$$

the routhian is expressed by

$$R = H - \boldsymbol{\beta}_{\text{rot}} \cdot \mathbf{p} - \frac{\hbar}{2}\boldsymbol{\Omega} \cdot \boldsymbol{\sigma} \equiv H - \boldsymbol{\Omega} \cdot (\boldsymbol{\ell} + \mathbf{s}), \quad (5)$$

which is the well known cranking approximation.

Using Skyrme interaction, the routhian expectation value for a Slater determinant can be written as the integral over the whole space

$$\langle R \rangle = \int \left(\mathcal{H}(\mathbf{r}) - \hbar\boldsymbol{\beta} \cdot \mathbf{j} - \frac{\hbar}{2}\boldsymbol{\Omega} \cdot \boldsymbol{\rho} \right) d\mathbf{r} \quad (6)$$

where \mathcal{H} is the energy density functional, \mathbf{j} is the current density and $\boldsymbol{\rho}$ is the spin-vector density whose expressions are given in Appendix A.1.

Minimizing this expectation value with respect to all single particle wave functions, one obtains the following expression for the one-body routhian (see Ref. [8] for instance)

$$\begin{aligned} h_q = & U_q - \frac{\hbar^2}{2m}\boldsymbol{\nabla}f_q \cdot \boldsymbol{\nabla} + \frac{i\hbar}{2}(\boldsymbol{\alpha}_q \cdot \boldsymbol{\nabla} + \boldsymbol{\nabla} \cdot \boldsymbol{\alpha}_q) \\ & - \hbar \left(\mathbf{S}_q + i\hbar\boldsymbol{\nabla}V_q^{\text{so}} \times \boldsymbol{\nabla} \right) \cdot \boldsymbol{\sigma}, \end{aligned} \quad (7)$$

where q stands for the considered charge state. The expressions of the various form factors entering this routhian are given in Appendix A.2.

2.2 Symmetries

As said in the introduction, we have chosen here to use axially symmetric harmonic oscillator wave functions for our basis states. Such wave functions have been widely used [9] to describe axially symmetric variational solutions. For the single particle hamiltonian, they entail symmetries with respect to the parity and the third component of the angular momentum, and can be written in the coordinates representation in terms of normalized Hermite and associated Laguerre polynomials H_{n_z} and $L_{n_r}^{|\Lambda|}$ (see Ref. [10]) as

$$\varphi_\mu(\mathbf{r}) = \left[\frac{\beta_z \beta_\perp^2}{\pi} e^{-(\xi^2 + \eta)} \right]^{1/2} e^{i\Lambda\theta} \eta^{|\Lambda|/2} H_{n_z}(\xi) L_{n_r}^{|\Lambda|}(\eta), \quad (8)$$

where μ represents the set $(n_z n_r \Lambda)$ of quantum numbers, β_z and β_\perp are the usual oscillator constants [9] which are generally related to the parameters $\beta_0 = (\beta_z \beta_\perp^2)^{1/3}$ and $q = (\beta_\perp / \beta_z)^2$ and ξ and η are given in terms of the cylindrical coordinates r and z by

$$\xi = z\beta_z, \quad \eta = r^2\beta_\perp^2. \quad (9)$$

For notational convenience, we will omit in the following the ξ and η dependence of the polynomials.

Whenever the time-reversal symmetry is broken, the third component of the angular momentum can no longer be chosen as a symmetry. It is well known however, that the Hartree–Fock hamiltonian obtained from the Skyrme interaction, the parity and for instance the first component of the signature operator [11] defined as

$$S_1 = \Pi_2 \Pi_3 \sigma_1, \quad (10)$$

(where Π_i is the reflection operator in the i direction, and σ_1 is the usual Pauli matrix) form a set of commuting operators. Imposing that the routhian also commutes with the two last symmetry operators limits the possible choice for β . As an example, if we restrict ourselves to first order polynomials in the coordinates, the vortical velocity field given by its components

$$\begin{aligned} \beta_1 &= 0, \\ \beta_2 &= ax_3, \\ \beta_3 &= bx_2 \end{aligned} \quad (11)$$

is the most general one that fulfills these commutation requirements. This analytical form corresponds to the so-called Riemann S -type ellipsoid solution presented by Chandrasekhar [12] in the context of fluid dynamics, whose application to nuclear physics has been discussed in particular in [6,13]. This field can then be rewritten as the sum of a global rotation term of angular velocity Ω and an intrinsic vorticity term of angular velocity ω both perpendicular to the first axis in the form

$$\begin{aligned}\beta_1 &= 0, \\ \beta_2 &= -(\Omega + \omega/q)x_3, \\ \beta_3 &= (\Omega + \omega q)x_2,\end{aligned}\tag{12}$$

where q is the a_3/a_2 axis ratio of the ellipsoid approximating the nuclear shape. The coupling of the rotation perpendicular to the first axis with the spins is taken into account by a term proportional to $\Omega\sigma_1$ in the routhian which still commutes with the signature operator.

Since the routhian single-particle eigenstates must have the same symmetries as the routhian, it is appropriate that the basis states are also eigenstates of the parity and signature operator. The action of the parity P and signature S_1 operator on axial harmonic oscillator states is given in usual notations by

$$P|n_z n_r \Lambda \Sigma\rangle = (-)^{n_z + \Lambda} |n_z n_r \Lambda \Sigma\rangle,\tag{13}$$

$$S_1|n_z n_r \Lambda \Sigma\rangle = (-)^{n_z} |n_z n_r - \Lambda - \Sigma\rangle,\tag{14}$$

from where we can see that S_1^2 is the identity operator, and thus the eigenvalues of S_1 are ± 1 . We then obtain eigenstates of the parity and signature in the form

$$|\mu s\rangle = \frac{\sqrt{2}}{2} \left[|\mu \frac{1}{2}\rangle + s(-)^{n_z} |\bar{\mu} - \frac{1}{2}\rangle \right], \quad s = \pm 1,\tag{15}$$

where μ ($\bar{\mu}$) represent the set (n_z, n_r, Λ) [$(n_z, n_r, -\Lambda)$] of quantum numbers, and we have

$$P|\mu s\rangle = (-)^{n_z + \Lambda} |\mu s\rangle, \quad S_1|\mu s\rangle = s|\mu s\rangle.\tag{16}$$

The single-particle eigenstates obtained after minimizing the routhian are written as

$$|k\rangle = \sum_{\mu} C_{\mu}^k |\mu s\rangle,\tag{17}$$

where the sum runs over basis states having the same eigenvalue for the two symmetry operators. In the coordinates representation, these eigenstates can

be decomposed in two components with spin $\frac{1}{2}$ and $-\frac{1}{2}$ as

$$\Phi_k(\mathbf{r}) = \Psi_k^+(\mathbf{r})|\frac{1}{2}\rangle + s\Psi_k^-(\mathbf{r})|-\frac{1}{2}\rangle, \quad (18)$$

and one deduces from equations (8) and (17)

$$\Psi_k^\pm(\mathbf{r}) = \left[\frac{\beta_z \beta_\perp^2}{2\pi} e^{-(\xi^2 + \eta)} \right]^{1/2} \sum_\mu (\pm)^{n_z} C_\mu^k e^{\pm i\Lambda\theta} \eta^{|\Lambda|/2} H_{n_z} L_{n_r}^{|\Lambda|}. \quad (19)$$

We are now able to calculate the expressions of the various densities of Appendix A.1. The density ρ of equation(A.7) for instance rewrites with the notations of (18) as

$$\rho = \sum_k \Psi_k^{+*} \Psi_k^+ + \Psi_k^{-*} \Psi_k^- \quad (20)$$

since $s^2 = 1$. Now inserting the expression (19) and rearranging the terms we get

$$\begin{aligned} \rho &= \frac{\beta_z \beta_\perp^2}{2\pi} e^{-(\xi^2 + \eta)} \sum_{\mu, \mu'} \left(\sum_k C_\mu^{k*} C_{\mu'}^k \right) \eta^{(|\Lambda| + |\Lambda'|)/2} H_{n_z} L_{n_r}^{|\Lambda|} H_{n'_z} L_{n'_r}^{|\Lambda'|} \\ &\quad \left(e^{i(\Lambda' - \Lambda)\theta} + (-)^{n_z + n'_z} e^{i(\Lambda - \Lambda')\theta} \right). \end{aligned} \quad (21)$$

The sum over k only involves the components C_μ^k of (17) and is nothing but the matrix element of the density matrix, that is

$$\sum_k C_\mu^{k*} C_{\mu'}^k = \rho_{\mu\mu'}. \quad (22)$$

In the general case this matrix is hermitian, but it can be shown [14] that the choice made for the basis states makes it a real symmetrical matrix. Using this property, the imaginary parts of the $\mu\mu'$ and $\mu'\mu$ terms in equation (21) cancel each other, and we can write

$$\begin{aligned} \rho &= \frac{\beta_z \beta_\perp^2}{2\pi} e^{-(\xi^2 + \eta)} \sum_{\mu, \mu'} \rho_{\mu\mu'} \eta^{(|\Lambda| + |\Lambda'|)/2} H_{n_z} L_{n_r}^{|\Lambda|} H_{n'_z} L_{n'_r}^{|\Lambda'|} \\ &\quad \cos[(\Lambda - \Lambda')\theta] \left(1 + (-)^{n_z + n'_z} \right). \end{aligned} \quad (23)$$

Finally, since the basis states $|\mu\rangle$ and $|\mu'\rangle$ have the same eigenvalue for the parity operator we can deduce from (16) that

$$(-)^{n_z + n'_z} = (-)^{\Lambda - \Lambda'}, \quad (24)$$

and the $\mu\mu'$ term of the sum (23) vanishes if the difference $\Lambda - \Lambda'$ is an odd integer. We then write at last the density ρ as

Table 1

Definition of the non-vanishing components of the Fourier series representing the various local densities in use; their parity π_z with respect to z is also given.

Densities	function	π_z
$\rho, \tau, \nabla^2 \rho, \nabla \cdot \mathbf{J}$	$\cos 2p\theta$	+
$j_r, \text{curl}_r \boldsymbol{\rho}$	$\sin[(2p+1)\theta]$	-
$j_\theta, \text{curl}_\theta \boldsymbol{\rho}, \text{curl}_z \mathbf{j}, \rho_z$	$\cos[(2p+1)\theta]$	-
$j_z, \text{curl}_z \boldsymbol{\rho}, \text{curl}_\theta \mathbf{j}, \rho_\theta$	$\sin[(2p+1)\theta]$	+
$\text{curl}_r \mathbf{j}, \rho_r$	$\cos[(2p+1)\theta]$	+

$$\rho = \frac{\beta_z \beta_\perp^2}{\pi} e^{-(\xi^2 + \eta)} \sum_{\mu, \mu'} \rho_{\mu\mu'} \eta^{(|\Lambda| + |\Lambda'|)/2} \delta_{\Lambda - \Lambda'}^{2p} \cos[(\Lambda - \Lambda')\theta] H_{n_z} H_{n'_z} L_{n_r}^{|\Lambda|} L_{n'_r}^{|\Lambda'|}. \quad (25)$$

with the definition

$$\delta_{\Lambda - \Lambda'}^{2p} = \begin{cases} 1 & \text{if } \Lambda - \Lambda' \text{ is an even integer,} \\ 0 & \text{if } \Lambda - \Lambda' \text{ is an odd integer.} \end{cases} \quad (26)$$

The calculations of the other local densities entering the one-body routhian are presented in Appendix B.1. It is clear from equation (25) and from the results of this Appendix that all the densities are obtained as real Fourier series in the angular variable θ . As some of the Fourier components of these densities are vanishing, we recall in Table 1 the non-vanishing components together with their parity with respect to the z variable. The maximal order of the non-vanishing components is $2\Lambda_{\max} + 1$ where Λ_{\max} is the higher Λ value among the basis states which is equal to N_0 in the case of a spherical basis and increases for deformed basis.

The form factors of the one-body routhian are expressed in Appendix A.2 as sums and products of these densities, non-integer powers of ρ and the Coulomb potential. We show in Appendix B.2 how the Coulomb potential can be obtained as a Fourier series in the θ variable, and the Fourier decompositions of the non-integer powers of ρ are obtained through weighted integrals over θ computed with a 48 points Gauss–Legendre quadrature formula. The Fourier

Table 2

Same as Table 1, but for the one-body routhian form factors.

Form factors	function	π_z
U, f, V^{so}	$\cos 2p\theta$	+
α_r	$\sin(2p+1)\theta$	-
α_θ, S_z	$\cos(2p+1)\theta$	-
α_z, S_θ	$\sin(2p+1)\theta$	+
S_r	$\cos(2p+1)\theta$	+

decomposition of β is readily obtained from equation (12) as

$$\begin{aligned}
 \beta_r &= z(\Omega + \omega q) \sin \theta, \\
 \beta_\theta &= -z(\Omega + \omega q) \cos \theta, \\
 \beta_z &= -r(\Omega + \omega/q) \sin \theta.
 \end{aligned}
 \tag{27}$$

Using the well known relations expressing products of trigonometrical functions as sums of trigonometrical functions of the sum and difference of their arguments, it is then straightforward to obtain the routhian form factors as Fourier series, whose non-vanishing components are given in Table 2.

Having expressed the routhian form factors as Fourier series in the angular variable allows us to calculate the routhian matrix elements as two-dimensional integrals, using simple selection rules. Indeed, if we write for instance, referring to Table 2, the scalar potential U as

$$U(\eta, \theta, \xi) = \sum_{n \geq 0} \cos(2n\theta) U^{(2n)}(\eta, \xi),
 \tag{28}$$

the part of the matrix element involving this form factor is spin diagonal and writes

$$\langle \mu s | U | \mu' s \rangle = \frac{1}{2} \sum_{n \geq 0} \langle \mu | \cos(2n\theta) U^{(2n)} | \mu' \rangle + (-)^{n_z + n'_z} \langle \bar{\mu} | \cos(2n\theta) U^{(2n)} | \bar{\mu}' \rangle,
 \tag{29}$$

readily performing the spin part of the scalar product. For a given n , the angular part of the first term on the right-hand side is simply proportional to

$$\int_0^{2\pi} e^{i(\Lambda' - \Lambda)\theta} \cos m\theta = \begin{cases} 0 & \text{if } m \neq |\Lambda - \Lambda'|, \\ \pi(1 + \delta_{|\Lambda - \Lambda'|}^0) & \text{if } m = |\Lambda - \Lambda'|, \end{cases}
 \tag{30}$$

and is identical to the angular part of the second term up to a complex conjugation. It can then be easily seen that equation (29) reduces to

$$\langle \mu s | U | \mu' s \rangle = \langle \mu \frac{1}{2} | \cos(|\Lambda - \Lambda'| \theta) U^{(|\Lambda - \Lambda'|)} | \mu' \frac{1}{2} \rangle, \quad (31)$$

which writes in analytical form

$$\langle \mu s | U | \mu' s \rangle = (1 + \delta_{\Lambda - \Lambda'}^0) \int_0^\infty d\eta \int_0^\infty d\xi e^{-(\xi^2 + \eta)} \eta^{(|\Lambda| + |\Lambda'|)/2} U^{(|\Lambda - \Lambda'|)} H_{n_z} H_{n'_z} L_{n_r}^{|\Lambda|} L_{n'_r}^{|\Lambda'|}, \quad (32)$$

where we have restricted the ξ integration to positive values, since the integrand is an even function of ξ . The calculation of the other terms of the routhian matrix elements also reduces to two-dimensional integrals and is presented in Appendix C. These integrations are performed through 10 points Gauss–Hermite and Gauss–Laguerre integrations (for the Gauss–Hermite integration, we use in fact a 20 points method which reduces to 10 points due to Π_3 symmetry properties). We therefore only need to compute the values of these densities and routhian form factors on the mesh points of a 10 by 10 grid.

2.3 Calculation of some observables

Within the Skyrme–Hartree–Fock formalism, the calculation of observables is generally reduced to a three-dimensional integral as is obviously the case for the routhian expectation value in equation (6). Expressing this integral as the integral of a Fourier series, only the first component needs to be integrated — which is done through a two-dimensional integral — since the integrals of the others are vanishing. For instance, the root mean square radius of the mass distribution which is given by

$$R_{\text{rms}}^2 = \frac{1}{A} \int \mathbf{r}^2 \rho(\mathbf{r}) d\mathbf{r} \quad (33)$$

where A is the total number of nucleons, reduces to the two-dimensional integral

$$R_{\text{rms}}^2 = \frac{4\pi}{A} \int_0^\infty r dr \int_0^\infty dz (r^2 + z^2) \rho^{(0)}(r, z), \quad (34)$$

since \mathbf{r}^2 does not depend upon θ . The quadrupole operator expectation value is easily obtained as

$$\langle Q_0 \rangle = 4\pi \int_0^\infty r dr \int_0^\infty dz (2z^2 - r^2) \rho^{(0)}(r, z), \quad (35)$$

similarly to what has been done for the root mean square radius calculation. The a_2 semi-axis length is given up to some normalization factors as the square root of $\langle x_2^2 \rangle$ written as

$$\langle x_2^2 \rangle = \frac{1}{A} \int r^2 \sin^2 \theta \rho(\mathbf{r}) \, d\mathbf{r}. \quad (36)$$

The integrand easily writes as a Fourier series upon developing $\sin^2 \theta$, and using the results of Table 1. Retaining only its first component, we get

$$\langle x_2^2 \rangle = \frac{2\pi}{A} \int_0^\infty r \, dr \int_0^\infty dz \, r^2 \left(\rho^{(0)}(r, z) - \frac{1}{2} \rho^{(2)}(r, z) \right). \quad (37)$$

And the expectation value of the non-axial quadrupole moment Q_{22} is obviously

$$\langle Q_{22} \rangle = A \langle x_2^2 - x_1^2 \rangle = -2\pi \int_0^\infty r \, dr \int_0^\infty dz \, r^2 \rho^{(2)}(r, z). \quad (38)$$

The first component of the total angular momentum is obtained from the current and spin-vector densities as

$$\langle L_1/\hbar \rangle = \langle (\mathbf{r} \times \mathbf{j} + \boldsymbol{\rho}) \cdot \mathbf{e}_1 \rangle, \quad (39)$$

where \mathbf{e}_1 is the unit vector in the first direction. It is expanded as

$$\langle L_1/\hbar \rangle = \int \left[r j_z \sin \theta - z(j_\theta \cos \theta + j_r \sin \theta) + \frac{1}{2}(\rho_r \cos \theta - \rho_\theta \sin \theta) \right] d\mathbf{r}, \quad (40)$$

and finally, referring to Table 1 we get,

$$\langle L_1/\hbar \rangle = \frac{2\pi}{A} \int_0^\infty r \, dr \int_0^\infty dz \left[r j_z^{(1)} - z(j_\theta^{(1)} + j_r^{(1)}) + \frac{1}{2}(\rho_r^{(1)} - \rho_\theta^{(1)}) \right]. \quad (41)$$

Taking into account the total angular momentum quantization rule for an even number of nucleons, we will only retain solutions that satisfy

$$\langle L_1/\hbar \rangle^2 = I(I + 1), \quad (42)$$

where I must be an even integer. The dynamical moment of inertia is calculated numerically as the first derivative of this angular momentum with respect to the angular velocity, namely

$$\mathfrak{S}^{(2)} = \frac{\partial I}{\partial \Omega}, \quad (43)$$

which, as mentioned by Gall et al. [15], provides a better numerical stability than the second derivative of the energy with respect to Ω .

3 Numerical tests

3.1 Convergence and computation time

Describing as we do here the single-particle states as a decomposition on a truncated harmonic oscillator basis, it is then crucial to study carefully the convergence of the solution with respect to the truncation. We are using the usual deformed truncation scheme, namely considering only as basis states those having an energy lower than what is obtained for a state with N_0 quanta of the equivalent spherical oscillator [9]. Discussions on this problem in the static case can be found in the literature [1]. We will thus concentrate here on the rotational case.

We have studied as an example rotating solutions of the nuclei ^{80}Sr . In Table 3 we present some properties of the $I = 20 \hbar$ solution for N_0 varying between 6 and 14 major shells. The deformation parameters were obtained from an optimization of the static solution. One sees that the routhian expectation value which is converged up to 10 eV (for a given basis size) vary by less than 0.23 percent as one adds two more shells. We have checked that the convergence of the various terms entering the routhian (eqs. A.2-A.6) also converge with such a good accuracy, with the noticeable exception of the time-odd contribution which is roughly 700 times smaller than the total routhian and varies by 5 percent between 8 and 10 shells. Now looking at the deformation properties, we see a rather nice convergence of the quadrupole moment above $N_0 = 8$. The variations of the non-axial quadrupole moment are of the same order in absolute values.

In the lower part of Table 3 we can see that the angular velocity varies by less

Table 3

Values of some observables in the $I = 20 \hbar$ solution of the nuclei ^{80}Sr as a function of N_0 (see Subsection 2.3 for calculation details). We used the parameters $\beta_0 = 0.534$ and $q = 1.2658$.

	6	8	10	12	14
$\langle R \rangle$ (MeV)	-686.69	-688.07	-688.75	-690.28	-690.61
$\langle Q_0 \rangle$ (b)	6.04	6.10	6.12	6.13	6.10
$\langle Q_{22} \rangle$ (b)	0.32	0.44	0.47	0.41	0.43
Ω (MeV)	0.831	0.831	0.831	0.836	0.832
$\mathfrak{S}^{(2)}$ ($\hbar^2 \cdot \text{MeV}^{-1}$)	24.46	24.06	23.96	23.93	23.91

Table 4

Computation time in seconds (measured on a HP9000/780 workstation), of one Hartree–Fock iteration within various formalisms as a function of N_0 . In the triaxial case, the first iteration is referred by ⁽¹⁾ and the following by ⁽²⁾.

	6	8	10	12	14
Vautherin’s formalism	0.24	0.59	1.46	3.07	5.98
“axial” case (parity, signature)	0.57	1.87	7.31	32.8	108
triaxial case ⁽¹⁾	9.65	15.6	28.8	68.5	169
triaxial case ⁽²⁾	1.49	4.69	15.2	52.1	150

than 0.5 percent as two shells are added. The convergence of the $\mathfrak{S}^{(2)}$ moment of inertia is even better, since its variation rate is constantly decreasing. This good convergence of the moment of inertia can be easily interpreted. Indeed, the moment of inertia is a differential quantity, and it is reasonable to expect small truncation effects for it in the near vicinity of a given solution.

Let us now discuss the computation time required by our formalism. First of all, we present in Table 4 the time needed to perform an iteration in the axial and the triaxial case, that is in the limiting case where only the first Fourier components are retained and in the case where all the non-vanishing components are used. In the triaxial case, we give the values for the first iteration where some initialization parameters are computed (see Appendix B.2) and for the following iterations which are shorter. We also present for comparison the computation time used by the static (and axial) formalism of Vautherin [9]. In static cases, the ratio between our formalism and Vautherin’s is somehow small for low N_0 values, but almost reaches 20 for $N_0 = 14$. This is due to our choice of the parity and signature symmetries for the single-particle states which only split each parity block into two, in contrast to Vautherin’s case. The time reversal symmetry breaking also doubles the size of the basis. On the contrary, excluding the initializations performed during the first iteration, the ratio between the triaxial and axial case in our formalism always decreases and stays relatively small.

An almost direct comparison of our code could be performed with the one built by Dobaczewski and Dudek [16] using a triaxial harmonic oscillator basis for the ^{152}Dy nucleus with the SkM* effective force. The basis size is defined by M of the order of 300 in their notation. This corresponds roughly to a deformation dependent truncation with $N_0 = 10$ in our notation. These authors quote a time of 9 seconds on a CRAY C90 for the vectorised version. They provide a factor of two to three to translate into the time used on e.g. an IBM RS/6000 station for a non vectorised version. The corresponding time in our calculation of ^{150}Gd with roughly the same basis size and after the first iteration, would

Table 5

Computation time in seconds of various parts of our formalism during the first iteration (measured on a HP9000/780 workstation). The last line gives an expectation of the time required by a fully triaxial formalism using triaxial wave functions.

	6	8	10	12	14
Diagonalization	0.08	0.48	3.19	22.4	83.2
Coulomb potential	8.17	10.9	13.6	16.4	19.1
Matrix elements and densities	1.05	3.63	10.6	25.8	56.4
Fully triaxial	13.7	40.1	113	289	661

be of less than 20 seconds which is of the order or slightly better than the quoted time.

Another way to estimate the advantages, or at least the competitiveness of our approach consists in extrapolating from our code the computation time required by triaxial basis calculations. For instance, in our case the routhian matrix element calculation involves two-dimensional integrations, where it would involve three-dimensional integrations in the fully triaxial case. Using 10 points Gauss-like integration method we can expect the matrix elements to be computed 10 times faster within our formalism. The same factor is expected for the densities calculation. In our formalism, each of the N_0 non-vanishing Fourier components of the Coulomb potential are calculated on a 10 by 10 mesh in the (r, z) plane performing a 10 by 10 integration in the (r', z') plane and a 48 points integration in the angular variable θ . In the fully triaxial case, it has to be computed for each of the points in the (x, y, z) mesh, each time performing a three-dimensional integral with 10 points. We thus expect our formalism to be roughly a factor $N_0/2$ slower than the fully triaxial case during the first iteration. The routhian diagonalization is also time-consuming but it should take the same amount of time within the two formalisms. Finally it seems that the computation of the energy and the routhian form factors should be slower in our formalism, but the time required for those calculations is negligible as compared to the overall execution time of an iteration.

All these remarks allow us to calculate an “expected” computation time for the fully triaxial formalism. We present this expectation in Table 5 together with the computation time of the discussed parts of our formalism. Comparing the last line of Tables 4 and 5, we see that our formalism is expected to be 4 times faster for $N_0 = 14$, and this factor is likely to be even larger for lower N_0 values, reaching a factor of 9 for $N_0 = 6$. These factors result of course only from a guess, and should be confirmed by existing fully triaxial codes.

Of practical interest also, would be a comparison between the computation times needed in our case and in other competing and totally different approaches to describe heavy nuclei within the same range of deformations. For the same ^{150}Gd nucleus at the same deformation (ground-state β value, $\gamma = 15^\circ$) and for the same basis size ($N_0 = 8$) and iteration number (30), the Bruyères le Châtel code (discarding the time needed to treat pairing correlations) would take [17] about 30 percent more time than our code. Of course, the Gogny effective force which is used there is completely different from our Skyrme force. Another point of comparison could be the 3D calculations of solutions having the same symmetries for slightly heavier deformed nuclei ($A \sim 190$) using the imaginary-time step technique where the computing time for a similar degree of convergence would be slightly larger [18] than ours. However it should be stressed that in their case the time used to treat pairing correlations has not been discarded.

It then appears that the orders of magnitude of the computing times for all considered codes, are identical with a slight advantage of our method in comparable approaches. It could be noted finally that the rather recent character of the present version of our code should reasonably leave some place for further optimization.

3.2 Results of superdeformed ^{150}Gd

We have chosen to test the physical results obtained within our formalism by comparison with the Hartree–Fock results of Bonche et al. [19] for the yrast band of the nucleus ^{150}Gd as calculated with the SkM* parameterization. Their formalism is based upon the computation of the one-body eigenstates on a three-dimensional mesh by solving the Schrödinger-like Hartree–Fock equation and thus are free from truncation effects but of course are contingent upon mesh size and related approximate numerical derivatives. The calculations presented here have been performed using 10 major shells. Though we should take into account at least the 21 lower order Fourier components of the densities, we have checked that the results are unchanged if we only use 7 Fourier components. This is due to the very little triaxiality of the solutions whose maximal triaxial axis ratio is only 1.02 (corresponding to $\gamma < 1^\circ$) and is reached at the end of the band.

The basis parameters optimization has been performed in several steps. We have obtained a first set of parameters from an optimization of a static solution constrained to the experimental value of the charge quadrupole moment of the yrast band. We have then minimized the routhian expectation values for rotating solutions with angular momentum ranging from 10 to $80 \hbar$ with steps of $5 \hbar$. Interpolating between these points, we obtained optimized parameters

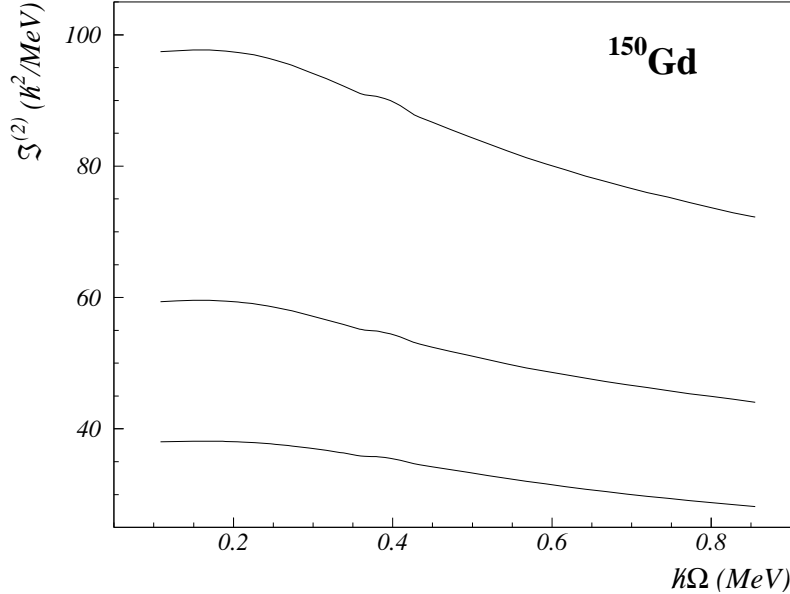


Fig. 1. Dynamical moment of inertia of the ^{150}Gd yrast band as a function of the angular velocity. The two curves at the bottom of the figure are the contribution of neutrons (upper curve) and protons (lower curve) to the moment of inertia.

with steps of $2 \hbar$.

We finally minimized the routhian for each of these quantized values of the angular momentum reaching an overall precision on the minimum of less than 0.1 keV. All these optimizations have been performed through successively minimizing quadratic fits of the routhian in the β_0 and q variables. We only performed calculations for angular momentum above $10 \hbar$ because we did not want here to describe the transition from superdeformation to normal deformation.

We show in Figs. 1 and 2 respectively the Dynamical moment of inertia and the charge quadrupole moment (calculated by replacing the matter density ρ in eq. (35) with the proton matter density ρ_p). While our values of the dynamical moment of inertia is in perfect agreement with the one depicted in [19], we obtain a charge quadrupole moment which is slightly larger by 0.2 e^2b . This effect cannot be related to truncation effects since we have checked that the same quadrupole moments are obtained with $N_0 = 14$. However, the variation of this moment over the yrast band is quantitatively well reproduced by our calculations.

We finally plot in Fig. 3 the neutron and proton single-particle routhians. We are globally in good agreement with the results of Ref. [19] (see for instance the proton gap for $Z = 66$ between the [651] and [411] states and the intruder orbital in the proton spectra appearing on top of the spectra above $\hbar\Omega =$

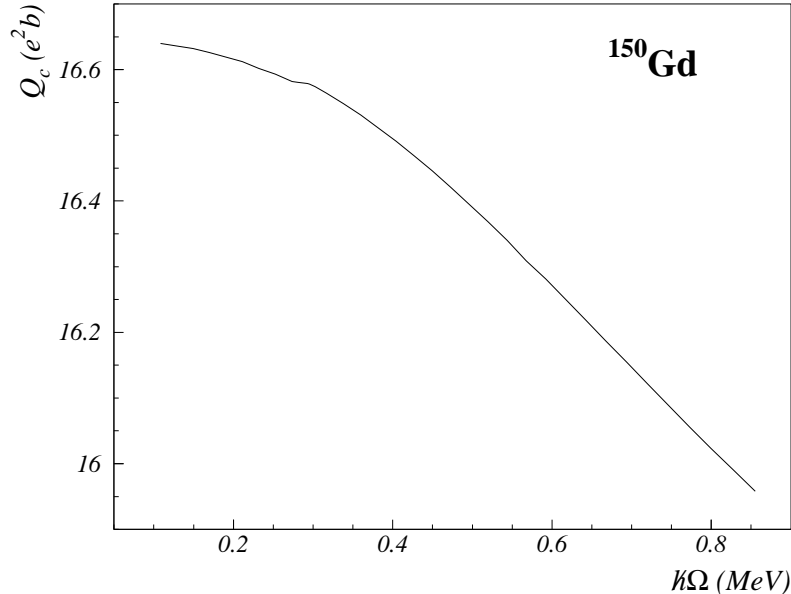


Fig. 2. Charge quadrupole moment of the ^{150}Gd yrast band as a function of the angular velocity.

0.5 MeV) but we observe some small differences. Among the less important are the labels of the eigenstates which are directly obtained in our formalism from the decompositions on the axial basis. In the neutron spectra, our $[521]3/2$ eigenstate (with a squared overlap of 60 percent) is labeled $[512]3/2$ by Bonche et al., and in the proton spectra, their $[532]5/2$ eigenstate is found to be in our formalism $[303]5/2$ (with a squared overlap of 81 percent) while the $[523]5/2$ state lies 500 keV below.

Comparing more closely the two results, the level spacings are seen to slightly differ, leading to different Ω values for some level crossings. In some cases, such small effects which we believe to be related to numerical methods in both cases can appear to be relevant, changing the properties of a given band. We have checked that these two effects do not depend on truncation effects by locally performing extended calculations with $N_0 = 14$.

4 S -type ellipsoids and superdeformed states in ^{150}Gd

We now wish to present some preliminary results obtained within the generalized routhian formalism. We use the velocity field of eq. (12) which couples the global rotation of the nucleus with an intrinsic vortical field and is known after Riemann and Chandrasekhar [12] as the S -type ellipsoid approximation. In this particular case the expression (3) of the routhian can be developed

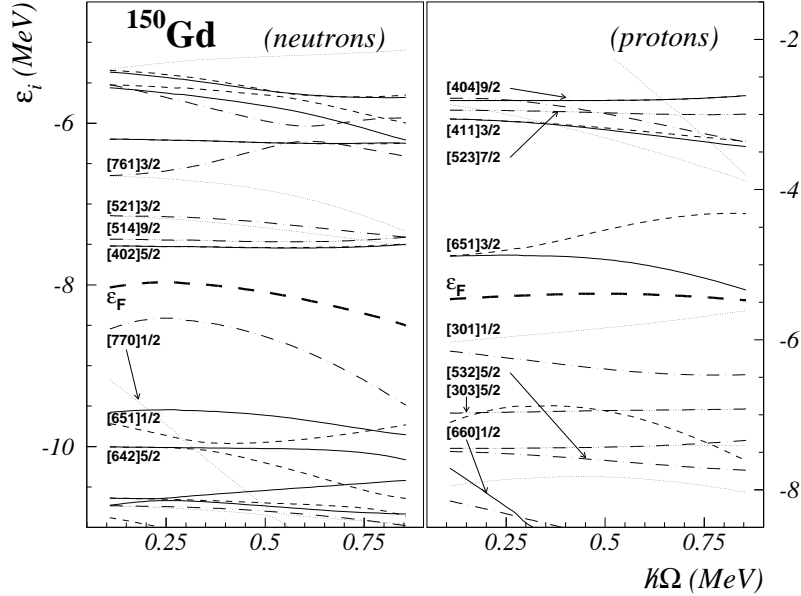


Fig. 3. Single-particle routhian spectra in the ^{150}Gd yrast band for both protons and neutrons. The convention used for the (parity,signature) representation is the following: (+,+) in full lines, (+,-) in dashed lines, (-,+) in dash-dotted lines and(-,-) in dotted lines.

through straightforward calculations as the doubly constrained operator

$$R = H - \Omega(L_1 + s_1) - \omega K_1, \quad (44)$$

where K_1 is the first component of the Kelvin circulation operator which writes in cartesian coordinates

$$K_1 = -i\hbar \left(q x_2 \frac{\partial}{\partial x_3} - \frac{1}{q} x_3 \frac{\partial}{\partial x_2} \right), \quad (45)$$

q being the axis ratio a_3/a_2 defined in Section 2.2. This definition corresponds to a double stretching of the angular momentum operator in both positions and momenta.

The introduction of the S -type velocity field in the context of nuclear physics has been already discussed by two of the authors and I. N. Mikhaïlov in Refs. [6,13]. In particular it has been stated that the Kelvin circulation defined above, which turns out to be the conjugate variable associated with the angle whose time derivative is called ω , should be quantized as is the angular momentum associated to the rotation angular velocity Ω . This quantization effect has been proposed as a tentative explanation of the striking $2\hbar$ staggering phenomenon observed in some superdeformed bands in the $A = 150$ mass region [20] and less clearly in the $A = 130$ mass region for Cerium isotopes [21].

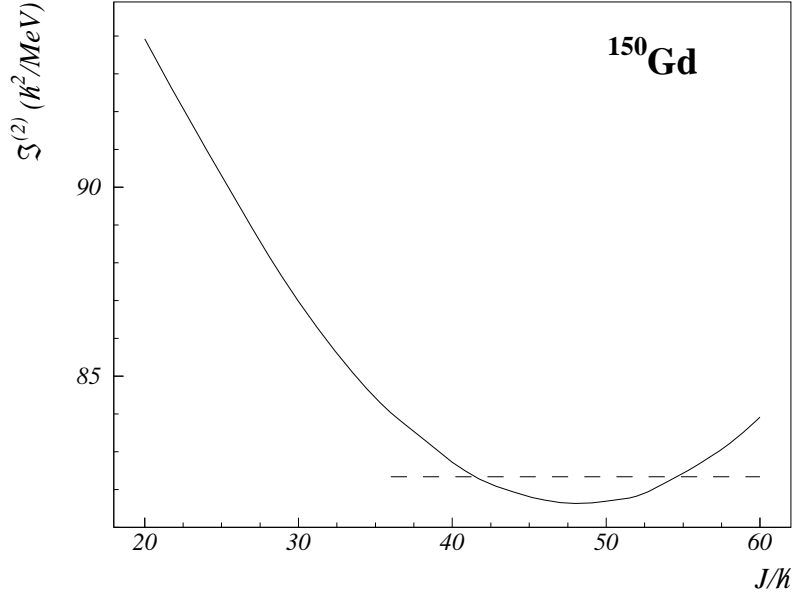


Fig. 4. Dynamical moment of inertia of $I = 50 \hbar$ solutions of the nuclei ^{150}Gd as a function of the Kelvin circulation J . The dashed line represent the yrast value of the moment of inertia. In all the calculations reported here we have used the basis parameters optimized for the yrast $I = 50 \hbar$ solution.

The expectation value of the Kelvin circulation is easily obtained from the expression (41) of the total angular momentum by performing the stretching in coordinates and momenta and removing the spin degrees of freedom contribution, as

$$\langle K_1/\hbar \rangle = \frac{2\pi}{A} \int_0^\infty r dr \int_0^\infty dz \left[\frac{r}{q} j_z^{(1)} - qz(j_\theta^{(1)} + j_r^{(1)}) \right]. \quad (46)$$

The quantization rule for the Kelvin circulation writes

$$\langle K_1/\hbar \rangle^2 = J(J+1), \quad (47)$$

where J must be an even integer due to the C2-symmetry character of the solution.

Upon varying the Kelvin circulation from its yrast value (which corresponds to a vanishing ω value), it is possible to obtain a wide class of collective flows, including irrotational flow, shear modes and others, corresponding to various moments of inertia differing from the one obtained on the yrast line. Such effects being also observed whenever pairing correlations are introduced, we can thus simulate the consequences of pairing forces in terms of current patterns by shifting the Kelvin circulation from its yrast value through the second dynamical constraint $-\omega K_1$.

To illustrate this point, we present in Fig. 4 the variation of the dynamical

moment of inertia as a function of J for ^{150}Gd solutions with $I = 50 \hbar$ (corresponding to $\hbar\Omega = 0.544$ MeV on the yrast line). The moment of inertia is seen to fit rather nicely on a parabola and can vary above and below the yrast value as J is varied. More precisely, classifying the solutions by the rigidity r of their flow patterns defined [22] as

$$r = 1 + \frac{\omega}{2\Omega}(q + 1/q), \quad (48)$$

where $r = 0$ corresponds to purely irrotational flow and $r = 1$ corresponds to global rotation, we can roughly associate the higher moments of inertia with $r < 1$ and the lower ones with $r > 1$. It is well known, as shown for instance by Durand et al. in Ref. [23] that the introduction of pairing forces leads to irrotational-like current lines. It is then very promising to notice that in the case of ^{150}Gd both pairing correlations (as shown in Ref. [19]) and $r < 1$ S -type solutions correspond to a higher moment of inertia than the yrast (Hartree–Fock) value.

We will not enter much into details here, leaving for a future publication [24] a more complete discussion on this subject. Let us merely mention that the Kelvin circulation value required to obtain a moment of inertia close to the experimental value which is around $90 \hbar^2/\text{MeV}$ in the $\hbar\Omega \sim 0.55$ MeV region is $J \sim 25 \hbar$. Such a value corresponds to a ratio $J/I = 2$ which is, in the hypothesis of Ref. [13], a condition required for a $2 \hbar$ staggering to appear.

5 Conclusions

The aim of this paper was to present a new formalism for solving the Skyrme–Hartree–Fock problem in the case of a generalized routhian which breaks both time reversal and axial symmetries. Even though such a kind of formalism was already existing as we recalled in the introduction, previous works have only described rotating solutions (i.e. being restricted to the single usual cranking case). More importantly, the choice here made to use axially symmetric basis states, has been shown to reduce the computation time with respect to the usual choice of triaxial basis states. The results of our formalism in the cranking case have been tested against the results available in the literature in the $A = 150$ mass region. They are in quite satisfactory agreement for usually considered observables in superdeformed nuclei.

We have also performed preliminary calculations within the S -type ellipsoid approximation. In Ref. [6], we had tackled the problem in the limiting case where the mean field is mocked-up by an harmonic potential. Here we started to lift up this approximation. However, this study is by no means complete and will be investigated in more details in forthcoming publications. It al-

ready gives us some hints, however, about the strong connection existing, as predicted, between the pairing correlations and the intrinsic vortical collective modes. For this purpose, it is clearly required that our formalism be extended to include pairing correlations even though some important results can certainly be obtained already within the Hartree–Fock approximation. This work is in progress, as we are currently working in upgrading our formalism to an Hartree–Fock–Bogoliubov approach, using a zero-range pairing force, treating moreover the complicated problem of projection on good particle number in the approximate and widely used Lipkin–Nogami scheme (see e.g. [25] for the implementation of this scheme in the framework of self-consistent calculations). Such a HFB formalism will also be instrumental in testing the hypothesis of Ref. [13] on the appearance of a $2\hbar$ staggering in some superdeformed bands. Indeed, since the moment of inertia renormalization induced by the pairing force is accompanied by a more pronounced irrotational character of the current patterns, the Kelvin circulation spectra along the yrast line should be very different in the HF and HFB cases. One should not therefore consider the J/I value in the pure Hartree–Fock case as the final word and rather consider it as a good starting point for a more comprehensive study of high spin nuclear dynamics.

Acknowledgments

This work which originates from one of the author’s (D. S.) PhD thesis has benefited from numerous fruitful and illuminating discussions with J. Meyer which we want to thank here. We are also deeply indebted to I. N. Mikhailov who participated with two of the authors (D. S. and P. Q.) in the development of the generalized routhian formalism in use in this paper and of the physics of nuclear intrinsic vortical currents. We are also grateful to J. Libert and J. Dudek who have been very helpful in allowing us to compare our computing time with those of other existing approaches.

A Routhians

A.1 Skyrme energy functional and local densities

The energy functional in the case of time-reversal symmetry breaking writes as [8]

$$\mathcal{H}(\mathbf{r}) = \mathcal{H}_{\text{kin}}(\mathbf{r}) + \mathcal{H}_{\text{vol}}(\mathbf{r}) + \mathcal{H}_{\text{so}}(\mathbf{r}) + \mathcal{H}_{\text{odd}}(\mathbf{r}) + \mathcal{H}_{\text{coul}}(\mathbf{r}), \quad (\text{A.1})$$

where these different terms are given below, omitting their \mathbf{r} dependence. The kinetic energy part writes

$$\mathcal{H}_{\text{kin}} = \frac{A-1}{A} \frac{\hbar^2}{2m} \tau, \quad (\text{A.2})$$

taking approximately into account the center of mass energy correction. The rest is given in terms of the force parameters B_i ($i = 1, 11$) given in Ref. [26]

$$\begin{aligned} \mathcal{H}_{\text{vol}} = & B_1 \rho^2 + B_2 \sum_q \rho_q^2 + B_7 \rho^{\alpha+2} + B_8 \rho^\alpha \sum_q \rho_q^2 \\ & + B_3 \rho \tau + B_4 \sum_q \rho_q \tau_q + B_5 \rho \nabla^2 \rho + B_6 \sum_q \rho_q \nabla^2 \rho_q, \end{aligned} \quad (\text{A.3})$$

$$\mathcal{H}_{\text{so}} = B_9 \left(\rho \nabla \cdot \mathbf{J} + \sum_q \rho_q \nabla \cdot \mathbf{J}_q \right), \quad (\text{A.4})$$

$$\begin{aligned} \mathcal{H}_{\text{odd}} = & B_9 \left(\nabla \times \rho \cdot \mathbf{j} + \sum_q \nabla \times \rho_q \cdot \mathbf{j}_q \right) - B_3 \mathbf{j}^2 - B_4 \sum_q \mathbf{j}_q^2 \\ & + B_{12} \rho^\alpha \rho^2 + B_{13} \rho^\alpha \sum_q \rho_q^2 + B_{10} \rho^2 + B_{11} \sum_q \rho_q^2, \end{aligned} \quad (\text{A.5})$$

in which some small contributions have been neglected as was discussed in [26] and

$$\mathcal{H}_{\text{coul}} = \frac{1}{2} e^2 \rho_p \int \frac{\rho_p(\mathbf{r}')}{|\mathbf{r} - \mathbf{r}'|} d\mathbf{r}' - \frac{3e^2}{4} \left(\frac{3}{\pi} \right)^{1/3} \rho_p^{4/3} \quad (\text{A.6})$$

using the Slater approximation [27] for the exchange term whose accuracy has been checked in Ref [28]. These expressions make use of the following local densities

$$\rho_q = \sum_k \Phi_k^* \Phi_k, \quad (\text{A.7})$$

$$\tau_q = \sum_k \nabla \Phi_k^* \cdot \nabla \Phi_k, \quad (\text{A.8})$$

$$\nabla \cdot \mathbf{J}_q = -i \sum_k \nabla \Phi_k^* \cdot \nabla \times \sigma \Phi_k \quad (\text{A.9})$$

$$\mathbf{j}_q = \frac{1}{2i} \sum_k \Phi_k^* \nabla \Phi_k - \Phi_k \nabla \Phi_k^*, \quad (\text{A.10})$$

$$\rho_q = \sum_k \Phi_k^* \sigma \Phi_k, \quad (\text{A.11})$$

where all the sums run over the occupied states for a given charge state q . When no charge index is present, we refer to the total density like e.g.

$$\rho = \sum_q \rho_q \quad (\text{A.12})$$

A.2 Form factors of the one-body routhian

The form factors appearing in eq. (7) are expressed as follows:

$$\begin{aligned} U_q = & 2(B_1\rho + B_2\rho_q) + (B_3\tau + B_4\tau_q) + 2(B_5\Delta\rho + B_6\Delta\rho_q) \\ & + (2 + \alpha)B_7\rho^{1+\alpha} + B_8\rho^{\alpha-1} \left(2\rho\rho_q + \alpha \sum_q \rho_q^2 \right) + B_9(\nabla \cdot \mathbf{J} + \nabla \cdot \mathbf{J}_q) \\ & + \alpha\rho^{\alpha-1} \left(B_{12}\boldsymbol{\rho}^2 + B_{13} \sum_q \boldsymbol{\rho}_q^2 \right) + \delta_{qp} \left(V_{\text{coul}}^{\text{dir}} - e^2 \left[\frac{3}{\pi} \rho_p \right]^{1/3} \right), \end{aligned} \quad (\text{A.13})$$

$$f_q = 1 + \frac{2m}{\hbar} (B_3\rho + B_4\rho_q), \quad (\text{A.14})$$

$$\hbar\boldsymbol{\alpha}_q = \hbar\boldsymbol{\beta} + 2(B_3\mathbf{j} + B_4\mathbf{j}_q) - B_9(\nabla \times \boldsymbol{\rho} + \nabla \times \boldsymbol{\rho}_q), \quad (\text{A.15})$$

$$\begin{aligned} \hbar\mathbf{S}_q = & \frac{\hbar}{2}\boldsymbol{\Omega} - B_9(\nabla \times \mathbf{j} + \nabla \times \mathbf{j}_q) - 2(B_{10}\boldsymbol{\rho} + B_{11}\boldsymbol{\rho}_q) \\ & - 2\rho^\alpha(B_{12}\boldsymbol{\rho} + B_{13}\boldsymbol{\rho}_q), \end{aligned} \quad (\text{A.16})$$

$$V_q^{\text{so}} = -\frac{B_9}{\hbar^2}(\rho + \rho_q), \quad (\text{A.17})$$

and

$$V_{\text{coul}}^{\text{dir}} = -e^2 \int \frac{\rho_p(\mathbf{r}')}{|\mathbf{r} - \mathbf{r}'|} d\mathbf{r}'. \quad (\text{A.18})$$

B Expression in the space coordinates of densities and energy form factors

B.1 Densities calculation

The calculation of the densities and routhian matrix elements requires the knowledge of the derivatives of those functions with respect to the three cylindrical coordinates. The derivation with respect to θ is straightforward from equation (19), whereas the other derivatives are given with obvious notations by

$$\partial_r \Psi^\pm(\mathbf{r}) = \left[\frac{\beta_z \beta_\perp^4}{2\pi} e^{-(\xi^2 + \eta)} \right]^{1/2} \sum_\mu (\pm)^{n_z} C_\mu^k e^{\pm i \Lambda \theta} \eta^{(|\Lambda| - 1)/2} H_{n_z} \bar{L}_{n_r}^{|\Lambda|}, \quad (\text{B.1})$$

$$\partial_z \Psi^\pm(\mathbf{r}) = \left[\frac{\beta_z^3 \beta_\perp^2}{2\pi} e^{-(\xi^2 + \eta)} \right]^{1/2} \sum_\mu (\pm)^{n_z} C_\mu^k e^{\pm i \Lambda \theta} \eta^{|\Lambda|} \bar{H}_{n_z} L_{n_r}^{|\Lambda|}, \quad (\text{B.2})$$

using as was done in Ref. [9] the definitions

$$\bar{H}_{n_z}(\xi) = \xi H_{n_z}(\xi) - H_{n_z+1}(\xi), \quad (\text{B.3})$$

$$\bar{L}_{n_r}^{|\Lambda|}(\eta) = 2(n_r + 1) L_{n_r+1}^{|\Lambda|}(\eta) - (2n_r + |\Lambda| + 2 - \eta) L_{n_r}^{|\Lambda|}(\eta). \quad (\text{B.4})$$

From the expressions given by Vautherin (eqs. (5.5) of Ref. [9]) for the τ and $\nabla^2 \rho$ densities in the case of time-reversal symmetry and the calculation of ρ performed in sect. 2.2 we can easily obtain in our case the following expressions:

$$\begin{aligned} \tau &= \frac{\beta_z \beta_\perp^2}{\pi} e^{-(\xi^2 + \eta)} \sum_{\mu, \mu'} \rho_{\mu\mu'} \eta^{(|\Lambda| + |\Lambda'|)/2 - 1} \delta_{\Lambda - \Lambda'}^{2p} \cos[(\Lambda - \Lambda')\theta] \\ &\quad \left\{ \eta \beta_z^2 \bar{H}_{n_z} \bar{H}_{n'_z} L_{n_r}^{|\Lambda|} L_{n'_r}^{|\Lambda'|} + \beta_\perp^2 H_{n_z} H_{n'_z} \left[\bar{L}_{n_r}^{|\Lambda|} \bar{L}_{n'_r}^{|\Lambda'|} + \Lambda \Lambda' L_{n_r}^{|\Lambda|} L_{n'_r}^{|\Lambda'|} \right] \right\}, \quad (\text{B.5}) \end{aligned}$$

$$\begin{aligned} \nabla^2 \rho &= 2\tau_q \frac{2\beta_z \beta_\perp^2}{\pi} e^{-(\xi^2 + \eta)} \sum_{\mu, \mu'} \rho_{\mu\mu'} \eta^{(|\Lambda| + |\Lambda'|)/2} \delta_{\Lambda - \Lambda'}^{2p} \cos[(\Lambda - \Lambda')\theta] \\ &\quad \left\{ \beta_z^2 \left[\xi^2 - 2(n_z + \frac{1}{2}) \right] + \beta_\perp^2 \left[\eta - 2(2n_r + |\Lambda| + 1) \right] \right\} \\ &\quad H_{n_z} H_{n'_z} L_{n_r}^{|\Lambda|} L_{n'_r}^{|\Lambda'|}. \quad (\text{B.6}) \end{aligned}$$

Using the expression (3.7) of Ref. [9] for the cylindrical components of the operator $\nabla \times \boldsymbol{\sigma}$, we obtain here the divergence of the spin-orbit density as

$$\begin{aligned}
\nabla \cdot \mathbf{J} = & 2 \sum_k \Im \left\{ \partial_r \Psi_k^{+*} \frac{1}{r} \partial_\theta \Psi_k^+ - \partial_r \Psi_k^{-*} \frac{1}{r} \partial_\theta \Psi_k^- \right\} \\
& + \Im \left\{ s \left(e^{-i\theta} \frac{1}{r} \partial_\theta \Psi_k^{+*} \partial_z \Psi_k^- + e^{i\theta} \frac{1}{r} \partial_\theta \Psi_k^{-*} \partial_z \Psi_k^+ \right) \right\} \\
& + \Re \left\{ s \left(e^{-i\theta} \partial_r \Psi_k^{+*} \partial_z \Psi_k^- - e^{i\theta} \partial_r \Psi_k^{-*} \partial_z \Psi_k^+ \right) \right\}, \tag{B.7}
\end{aligned}$$

where $\Re\{x\}$ ($\Im\{x\}$ resp.) represents the real part (imaginary part resp.) of x . This expression may be worked out with the help of the equations (19), (B.1) and (B.2) as

$$\begin{aligned}
\nabla \cdot \mathbf{J} = & \frac{\beta_z \beta_\perp^2}{\pi} e^{-(\xi^2 + \eta)} \sum_{\mu, \mu'} \rho_{\mu\mu'} \eta^{(|\Lambda| + |\Lambda'|)/2} \\
& \beta_\perp^2 \eta^{-1} \Lambda' H_{n_z} H_{n'_z} \bar{L}_{n_r}^{|\Lambda|} L_{n'_r}^{|\Lambda'|} \cos[(\Lambda - \Lambda')\theta] \left(1 + (-)^{n_z + n'_z} \right) \\
& - s \beta_z \beta_\perp \eta^{-1/2} H_{n_z} \bar{H}_{n'_z} \Lambda L_{n_r}^{|\Lambda|} L_{n'_r}^{|\Lambda'|} \cos[(\Lambda + \Lambda' + 1)\theta] \left((-)^{n'_z} - (-)^{n_z} \right) \\
& + s \beta_z \beta_\perp \eta^{-1/2} H_{n_z} \bar{H}_{n'_z} \bar{L}_{n_r}^{|\Lambda|} L_{n'_r}^{|\Lambda'|} \cos[(\Lambda + \Lambda' + 1)\theta] \left((-)^{n'_z} - (-)^{n_z} \right). \tag{B.8}
\end{aligned}$$

Now introducing the definition

$$\delta_{\Lambda - \Lambda'}^{2p+1} = \begin{cases} 1 & \text{if } \Lambda - \Lambda' \text{ is an odd integer,} \\ 0 & \text{if } \Lambda - \Lambda' \text{ is an even integer,} \end{cases} \tag{B.9}$$

we finally write this density in the following way:

$$\begin{aligned}
\nabla \cdot \mathbf{J} = & \frac{2\beta_z \beta_\perp^3}{\pi} e^{-(\xi^2 + \eta)} \sum_{\mu, \mu'} \rho_{\mu\mu'} \eta^{(|\Lambda| + |\Lambda'| - 1)/2} \\
& \Lambda' \beta_\perp \eta^{-1/2} H_{n_z} H_{n'_z} \bar{L}_{n_r}^{|\Lambda|} L_{n'_r}^{|\Lambda'|} \delta_{\Lambda - \Lambda'}^{2p} \cos[(\Lambda - \Lambda')\theta] \\
& + s (-)^{n'_z} \beta_z H_{n_z} \bar{H}_{n'_z} L_{n_r}^{|\Lambda|} \left(\bar{L}_{n_r}^{|\Lambda|} - \Lambda L_{n_r}^{|\Lambda|} \right) \delta_{\Lambda - \Lambda'}^{2p+1} \cos[(\Lambda + \Lambda' + 1)\theta]. \tag{B.10}
\end{aligned}$$

From the definition (A.10) of the current density, one can write the r component of this density like

$$j_r = \sum_k \Im \left\{ \Psi_k^{+*} \partial_r \Psi_k^+ + \Psi_k^{-*} \partial_r \Psi_k^- \right\}, \tag{B.11}$$

which can be readily developed as

$$\begin{aligned}
j_r = & \frac{\beta_z \beta_\perp^2}{2\pi} e^{-(\xi^2 + \eta)} \sum_{\mu, \mu'} \rho_{\mu\mu'} \eta^{(|\Lambda| + |\Lambda'|)/2} \beta_\perp \eta^{-1/2} H_{n_z} H_{n'_z} L_{n_r}^{|\Lambda|} \bar{L}_{n'_r}^{|\Lambda'|} \\
& \sin[(\Lambda' - \Lambda)\theta] \left(1 - (-)^{n_z + n'_z} \right), \tag{B.12}
\end{aligned}$$

since the sine is an odd function. This expression can be simplified as

$$j_r = -\frac{\beta_z \beta_\perp^3}{\pi} e^{-(\xi^2 + \eta)} \sum_{\mu, \mu'} \rho_{\mu\mu'} \eta^{(|\Lambda| + |\Lambda'| - 1)/2} \delta_{\Lambda - \Lambda'}^{2p+1} \sin[(\Lambda - \Lambda')\theta] H_{n_z} H_{n'_z} L_{n_r}^{|\Lambda|} \bar{L}_{n'_r}^{|\Lambda'|}. \quad (\text{B.13})$$

In the same way, the two other components of this density are expressed as

$$j_\theta = \frac{\beta_z \beta_\perp^3}{\pi} e^{-(\xi^2 + \eta)} \sum_{\mu, \mu'} \rho_{\mu\mu'} \eta^{(|\Lambda| + |\Lambda'| - 1)/2} \delta_{\Lambda - \Lambda'}^{2p+1} \cos[(\Lambda - \Lambda')\theta] \Lambda' H_{n_z} H_{n'_z} L_{n_r}^{|\Lambda|} \bar{L}_{n'_r}^{|\Lambda'|}, \quad (\text{B.14})$$

$$j_z = -\frac{\beta_z^2 \beta_\perp^2}{\pi} e^{-(\xi^2 + \eta)} \sum_{\mu, \mu'} \rho_{\mu\mu'} \eta^{(|\Lambda| + |\Lambda'| - 1)/2} \delta_{\Lambda - \Lambda'}^{2p+1} \sin[(\Lambda - \Lambda')\theta] H_{n_z} \bar{H}_{n'_z} L_{n_r}^{|\Lambda|} L_{n'_r}^{|\Lambda'|}. \quad (\text{B.15})$$

To calculate the spin-vector density, we will use the cylindrical coordinates of the operator σ which are given in terms of the Pauli matrices by

$$\begin{aligned} \sigma_r &= \frac{1}{2} (\sigma_+ e^{-i\theta} + \sigma_- e^{i\theta}), \\ \sigma_\theta &= -\frac{i}{2} (\sigma_+ e^{-i\theta} - \sigma_- e^{i\theta}), \end{aligned} \quad (\text{B.16})$$

the z component being evident. We can then write

$$\rho_r = 2 \sum_k \Re \left\{ s \Psi_k^{+*} \Psi_k^- e^{-i\theta} \right\}, \quad (\text{B.17})$$

$$\rho_\theta = 2 \sum_k \Im \left\{ s \Psi_k^{+*} \Psi_k^- e^{-i\theta} \right\}, \quad (\text{B.18})$$

$$\rho_z = \sum_k \Psi_k^{+*} \Psi_k^+ - \Psi_k^{-*} \Psi_k^-. \quad (\text{B.19})$$

It is then straightforward to obtain

$$\rho_r = \frac{\beta_z \beta_\perp^2}{\pi} e^{-(\xi^2 + \eta)} \sum_{\mu, \mu'} s(-)^{n'_z} \rho_{\mu\mu'} \eta^{(|\Lambda| + |\Lambda'|)/2} \delta_{\Lambda - \Lambda'}^{2p} \cos[(\Lambda + \Lambda' + 1)\theta] H_{n_z} H_{n'_z} L_{n_r}^{|\Lambda|} L_{n'_r}^{|\Lambda'|}, \quad (\text{B.20})$$

since the sum of the $\mu\mu'$ and $\mu'\mu$ terms cancel when $n_z + n'_z$ is an odd integer. The θ component is simply given by

$$\rho_\theta = -\frac{\beta_z \beta_\perp^2}{\pi} e^{-(\xi^2 + \eta)} \sum_{\mu, \mu'} s(-)^{n'_z} \rho_{\mu\mu'} \eta^{(|\Lambda| + |\Lambda'|)/2} \delta_{\Lambda - \Lambda'}^{2p} \sin[(\Lambda + \Lambda' + 1)\theta] H_{n_z} H_{n'_z} L_{n_r}^{|\Lambda|} L_{n'_r}^{|\Lambda'|}, \quad (\text{B.21})$$

and since equations (B.19) and (20) only differ by a minus sign between the two terms of the right-hand side we have

$$\rho_z = \frac{\beta_z \beta_\perp^2}{\pi} e^{-(\xi^2 + \eta)} \sum_{\mu, \mu'} \rho_{\mu\mu'} \eta^{(|\Lambda| + |\Lambda'|)/2} \delta_{\Lambda - \Lambda'}^{2p+1} \cos[(\Lambda - \Lambda')\theta] H_{n_z} H_{n'_z} L_{n_r}^{|\Lambda|} L_{n'_r}^{|\Lambda'|}. \quad (\text{B.22})$$

The components of the curl of \mathbf{j} and $\boldsymbol{\rho}$ which also enter the one-body routhian can be obtained upon mixing partial derivatives in the following way:

$$\text{curl}_r \mathbf{j} = \partial_\theta j_z - \partial_z j_\theta, \quad (\text{B.23})$$

$$\text{curl}_\theta \mathbf{j} = \partial_z j_r - \partial_r j_z, \quad (\text{B.24})$$

$$\text{curl}_z \mathbf{j} = \partial_r j_\theta - \partial_\theta j_r + \frac{1}{r} j_\theta. \quad (\text{B.25})$$

B.2 Calculation of the Coulomb potential

It is well known and used in Ref. [9] that the Coulomb potential of equation (A.18) can be written after two integrations by part as

$$V_{\text{coul}}^{\text{dir}}(\mathbf{r}) = -\frac{e^2}{2} \int |\mathbf{r} - \mathbf{r}'| |\nabla^2 \rho_p(\mathbf{r}')| d\mathbf{r}'. \quad (\text{B.26})$$

Developing

$$|\mathbf{r} - \mathbf{r}'| = [(z - z')^2 + (r + r')^2]^{1/2} \left[1 - k^2 \cos^2 \left(\frac{\theta - \theta'}{2} \right) \right]^{1/2}, \quad (\text{B.27})$$

with

$$k^2 = \frac{4rr'}{(z - z')^2 + (r + r')^2}, \quad (\text{B.28})$$

and writing as suggested by Table 1

$$\nabla^2 \rho_p(\mathbf{r}') = \sum_{n \geq 0} D^{2n}(r', z') \cos 2n\theta', \quad (\text{B.29})$$

the Coulomb potential can be developed in the following way

$$V_{\text{coul}}^{\text{dir}}(\mathbf{r}) = \frac{e^2}{2} \sum_{n \geq 0} \int_0^\infty r' dr' \int_{-\infty}^\infty dz' \left[(z - z')^2 + (r + r')^2 \right]^{1/2} D^{2n}(r', z') \int_0^{2\pi} d\theta' \left[1 - k^2 \cos^2 \left(\frac{\theta - \theta'}{2} \right) \right]^{1/2} \cos 2n\theta'. \quad (\text{B.30})$$

In terms of $u = (\theta - \theta')/2$, the angular part of the above integral rewrites as

$$I^{2n} = 2 \int_0^\pi du \left(1 - k^2 \cos^2 u \right)^{1/2} \cos(4nu - 2n\theta). \quad (\text{B.31})$$

Developing the last cosine of this expression, we can factorize the θ dependence out of the integral and obtain

$$I^{2n} = 4 \cos 2n\theta \int_0^{\pi/2} du \left(1 - k^2 \cos^2 u \right)^{1/2} \cos 4nu, \quad (\text{B.32})$$

since the other term is vanishing. We can then write the Coulomb potential as a Fourier series in the θ variable:

$$V_{\text{coul}}^{\text{dir}}(\mathbf{r}) = 4e^2 \sum_{n \geq 0} \cos 2n\theta \int_0^\infty r' dr' \int_0^\infty dz' \left[(z - z')^2 + (r + r')^2 \right]^{1/2} D^{2n}(r', z') \int_0^{\pi/2} du \left(1 - k^2 \cos^2 u \right)^{1/2} \cos 4nu, \quad (\text{B.33})$$

where we have restricted the integral over z to positive values using parity properties. The r' and z' integrals are then performed numerically through 10 points Gauss–Hermite and Gauss–Laguerre quadrature formulas whereas the u integral is performed through a 48 points Gauss–Legendre quadrature formula during the first iteration, the results being then stored for future use.

C Calculations of routhian matrix elements

Comparing our expression (32) for the scalar part of the routhian matrix element with Vautherin’s equation (4.22) in Ref. [9], we can straightforwardly obtain the kinetic part of the matrix element as

$$\begin{aligned} \langle \mu s | \nabla f \cdot \nabla | \mu' s \rangle &= -(1 + \delta_{\Lambda - \Lambda'}^0) \int_0^\infty d\eta \int_0^\infty d\xi e^{-(\xi^2 + \eta)} \eta^{(|\Lambda| + |\Lambda'|)/2} \\ &\quad f^{(|\Lambda - \Lambda'|)} \left[\beta_\perp^2 \eta^{-1} H_{n_z} H_{n'_z} \left(\bar{L}_{n_r}^{|\Lambda|} \bar{L}_{n'_r}^{|\Lambda'|} + \Lambda \Lambda' L_{n_r}^{|\Lambda|} L_{n'_r}^{|\Lambda'|} \right) \right. \\ &\quad \left. + \beta_z^2 L_{n_r}^{|\Lambda|} L_{n'_r}^{|\Lambda'|} \bar{H}_{n_z} \bar{H}_{n'_z} \right], \end{aligned} \quad (\text{C.1})$$

where we use, as will be done throughout this Appendix, the notation $\Gamma^{(n)}$ to represent the n -th non-vanishing component of the Fourier series of any

routhian form factor Γ (see Table 2). The calculation of the $\boldsymbol{\alpha}$ part of the matrix element can be rewritten through an integration by parts as

$$\langle \mu s | (\boldsymbol{\alpha} \cdot \nabla + \nabla \cdot \boldsymbol{\alpha}) | \mu' s \rangle = \langle \mu s | \boldsymbol{\alpha} \cdot \nabla | \mu' s \rangle - \langle \mu' s | \boldsymbol{\alpha} \cdot \nabla | \mu s \rangle^*, \quad (\text{C.2})$$

which allows us to only calculate the first term on the right-hand side, the second term being easily deduced from it.

$$\begin{aligned} \langle \mu s | \boldsymbol{\alpha} \cdot \nabla | \mu' s \rangle &= \frac{1}{2} \sum_{n \geq 0} \left(\langle \mu | \cos[(2n+1)\theta] \alpha_\theta^{(2n+1)} \frac{\partial_\theta}{r} | \mu' \rangle \right. \\ &\quad \left. + \langle \mu | \sin[(2n+1)\theta] \left(\alpha_r^{(2n+1)} \partial_r + \alpha_z^{(2n+1)} \partial_z \right) | \mu' \rangle \right) \\ &\quad + (-)^{n_z+n'_z} [(\mu, \mu') \rightarrow (\bar{\mu}, \bar{\mu}')], \end{aligned} \quad (\text{C.3})$$

where the term $[(\mu, \mu') \rightarrow (\bar{\mu}, \bar{\mu}')]]$ represents a term identical to the previous one with $\bar{\mu}$ and $\bar{\mu}'$ replacing μ and μ' . Making use of equation (30) and of the following identity:

$$\int_0^{2\pi} e^{ik\theta} \sin m\theta = \begin{cases} 0 & \text{if } m \neq |k| \text{ and } m \neq 0, \\ i\pi \frac{k}{m} & \text{if } m = |k|, \end{cases} \quad (\text{C.4})$$

one can notice that the $\mu\mu'$ and $\bar{\mu}\bar{\mu}'$ contributions in equation (C.3) are identical. The sum over n therefore reduces to

$$\begin{aligned} \langle \mu s | \boldsymbol{\alpha} \cdot \nabla | \mu' s \rangle &= \langle \mu | \sin(|\Lambda - \Lambda'| \theta) \left(\alpha_r^{(|\Lambda - \Lambda'|)} \partial_r + \alpha_z^{(|\Lambda - \Lambda'|)} \partial_z \right) | \mu' \rangle \\ &\quad + \langle \mu | \cos[|\Lambda - \Lambda'| \theta] \alpha_\theta^{(|\Lambda - \Lambda'|)} \frac{\partial_\theta}{r} | \mu' \rangle, \end{aligned} \quad (\text{C.5})$$

which expands as

$$\begin{aligned} \langle \mu s | \boldsymbol{\alpha} \cdot \nabla | \mu' s \rangle &= i\beta_\perp \int_0^\infty d\eta \int_0^\infty d\xi e^{-(\xi^2 + \eta)} \eta^{(|\Lambda| + |\Lambda'| - 1)/2} H_{n_z} L_{n_r}^{|\Lambda|} \\ &\quad \left[\frac{\Lambda' - \Lambda}{|\Lambda' - \Lambda|} \left(\alpha_r^{(|\Lambda - \Lambda'|)} H_{n'_z} \bar{L}_{n'_r}^{|\Lambda'|} + \frac{\beta_z}{\beta_\perp} \eta^{1/2} \alpha_z^{(|\Lambda - \Lambda'|)} \bar{H}_{n'_z} L_{n'_r}^{|\Lambda'|} \right) \right. \\ &\quad \left. + \alpha_\theta^{(|\Lambda - \Lambda'|)} \Lambda' H_{n'_z} L_{n'_r}^{|\Lambda'|} \right] \end{aligned} \quad (\text{C.6})$$

The spin part of the matrix element involves a spin diagonal term and two spin anti-diagonal terms. Using the relations (B.16) and performing the spin part of the scalar product, they respectively write

$$\begin{aligned} \langle \mu s | S_z \sigma_z | \mu' s \rangle &= \frac{1}{2} \sum_{n \geq 0} \langle \mu | \cos[(2n+1)\theta] S_z^{(2n+1)} | \mu' \rangle \\ &\quad - (-)^{n_z + n'_z} \langle \bar{\mu} | \cos[(2n+1)\theta] S_z^{(2n+1)} | \bar{\mu}' \rangle, \end{aligned} \quad (\text{C.7})$$

$$\begin{aligned} \langle \mu s | S_r \sigma_r | \mu' s \rangle &= \frac{1}{2} \sum_{n \geq 0} s(-)^{n'_z} \langle \mu | e^{-i\theta} \cos[(2n+1)\theta] S_r^{(2n+1)} | \bar{\mu}' \rangle \\ &\quad + s(-)^{n_z} \langle \bar{\mu} | e^{i\theta} \cos[(2n+1)\theta] S_r^{(2n+1)} | \mu' \rangle, \end{aligned} \quad (\text{C.8})$$

and

$$\begin{aligned} \langle \mu s | S_\theta \sigma_\theta | \mu' s \rangle &= \frac{-i}{2} \sum_{n \geq 0} s(-)^{n'_z} \langle \mu | e^{-i\theta} \sin[(2n+1)\theta] S_\theta^{(2n+1)} | \bar{\mu}' \rangle \\ &\quad - s(-)^{n_z} \langle \bar{\mu} | e^{i\theta} [\sin(2n+1)\theta] S_\theta^{(2n+1)} | \mu' \rangle. \end{aligned} \quad (\text{C.9})$$

In all these three expressions again, the two terms on the right-hand side are the same and we finally obtain the expression

$$\begin{aligned} \langle \mu s | \mathbf{S} \cdot \boldsymbol{\sigma} | \mu' s \rangle &= \int_0^\infty d\eta \int_0^\infty d\xi e^{-(\xi^2 + \eta)} \eta^{(|\Lambda| + |\Lambda'|)/2} H_{n_z} H_{n'_z} L_{n_r}^{|\Lambda|} L_{n'_r}^{|\Lambda'|} \\ &\quad \left[S_z^{(|\Lambda - \Lambda'|)} + s(-)^{n_z} \left(S_r^{(|\Lambda + \Lambda' + 1|)} \right. \right. \\ &\quad \left. \left. - \frac{\Lambda + \Lambda' + 1}{|\Lambda + \Lambda' + 1|} S_\theta^{(|\Lambda + \Lambda' + 1|)} \right) \right]. \end{aligned} \quad (\text{C.10})$$

One can easily develop the spin-orbit term of the one-body routhian of eq. (7) as

$$\begin{aligned} U^{\text{so}} &= (\nabla V^{\text{so}} \times \nabla) \cdot \boldsymbol{\sigma} = (\partial_r V^{\text{so}}) \left(\frac{\partial_\theta}{r} \sigma_z - \partial_z \sigma_\theta \right) + \frac{1}{r} (\partial_\theta V^{\text{so}}) (\partial_z \sigma_r - \partial_r \sigma_z) \\ &\quad + (\partial_z V^{\text{so}}) \left(\partial_r \sigma_\theta - \frac{\partial_\theta}{r} \sigma_r \right). \end{aligned} \quad (\text{C.11})$$

As the calculation of the matrix element is rather long, we will not enter into details here. It has been established in Ref. [14] using the same technique as we used in this Appendix that, after integrating by parts to eliminate the $(\partial_i V^{\text{so}})$ terms, we get:

$$\begin{aligned}
\langle \mu s | U^{\text{so}} | \mu' s \rangle = & \beta_{\perp} \int_0^{\infty} d\eta \int_0^{\infty} d\xi e^{-(\xi^2 + \eta)} \eta^{(|\Lambda| + |\Lambda'|)/2 - 1} \left\{ \right. \\
& \beta_{\perp} (1 + \delta_{|\Lambda - \Lambda'|}^0) V_{\text{so}}^{(|\Lambda - \Lambda'|)} H_{n_z} H_{n'_z} \left[\Lambda L_{n_r}^{|\Lambda|} \bar{L}_{n'_r}^{|\Lambda'|} + \Lambda' \bar{L}_{n_r}^{|\Lambda|} L_{n'_r}^{|\Lambda'|} \right] \\
& - s(-)^{n_z} \beta_z \eta^{1/2} (1 + \delta_{|\Lambda + \Lambda' + 1|}) V_{\text{so}}^{(|\Lambda + \Lambda' + 1|)} \left[H_{n_z} \bar{H}_{n'_z} L_{n'_r}^{|\Lambda'|} \right. \\
& \left. \left. (\bar{L}_{n_r}^{|\Lambda|} - \Lambda L_{n_r}^{|\Lambda|}) - \bar{H}_{n_z} H_{n'_z} L_{n_r}^{|\Lambda|} (\bar{L}_{n'_r}^{|\Lambda'|} - \Lambda' L_{n'_r}^{|\Lambda'|}) \right] \right\} \quad (\text{C.12})
\end{aligned}$$

References

- [1] H. Flocard, P. Quentin, A. K. Kerman, and D. Vautherin, Nucl. Phys. A 203 (1973) 433.
- [2] J. L. Egido and L. M. Robledo, Phys. Rev. Lett. 70 (1993) 2876.
- [3] B. Girod, J.-P. Delaroche, J.-F. Berger, and J. Libert, Phys. Lett. B 325 (1994) 1.
- [4] J. Dobaczewski and J. Dudek, Phys. Rev. C 52 (1995) 1827.
- [5] J. Bartel, P. Quentin, M. Brack, C. Guet, and H. B. Haakansson, Nucl. Phys. A 386 (1982) 79.
- [6] I. N. Mikhaïlov, P. Quentin, and D. Samsen, Nucl. Phys. A 627 (1997) 259.
- [7] D. Samsen, P. Quentin, and I. N. Mikhaïlov, in preparation.
- [8] Y. M. Engel, D. M. Brink, K. Goeke, S. J. Krieger, and D. Vautherin, Nucl. Phys. A 249 (1975) 215.
- [9] D. Vautherin, Phys. Rev. C 7 (1973) 296.
- [10] M. Abramowitz and I. A. Stegun. *Handbook of Mathematical Functions*. Dover, New-York, 1965.
- [11] A. L. Goodman, Nucl. Phys. A 230 (1974) 466.
- [12] S. Chandrasekhar. *Ellipsoidal Figures of Equilibrium*. Dover, New-York, 1987.
- [13] I. N. Mikhaïlov and P. Quentin, Phys. Rev. Lett. 74 (1995) 3336.
- [14] D. Samsen. PhD thesis, Universit Bordeaux-I, 1997, unpublished.
- [15] B. Gall, P. Bonche, J. Dobaczewski, H. Flocard, and P. H. Heenen, Z. Phys. A 348 (1994) 183.
- [16] J. Dobaczewski and J. Dudek, Comp. Phys. Comm. 102 (1997) 166 ; 183
- [17] J. Libert, private communication.
- [18] J. Meyer, private communication.

- [19] P. Bonche, H. Flocard, and P. H. Heenen, Nucl. Phys. A 598 (1996) 169.
- [20] S. Flibotte et al., Phys. Rev. Lett. 71 (1993) 4229 ;
D. S. Haslip et al., Phys. Rev. Lett. 78 (1997) 3447.
- [21] A. T. Semple et al., Phys. Rev. Lett. 76 (1996) 3671.
- [22] G. Rosensteel, Phys. Rev. C 46 (1992) 1818.
- [23] M. Durand, P. Schuck, and J. Kunz, Nucl. Phys. A 439 (1985) 263.
- [24] D. Samsøen, P. Quentin, and I. N. Mikhaïlov, Phys. Rev. C, in press.
- [25] P. Quentin, N. Redon, J. Meyer, and M. Meyer, Phys. Rev. C 43 (1991) 361.
- [26] P. Bonche, H. Flocard, and P. H. Heenen, Nucl. Phys. A 467 (1987) 115.
- [27] P. Gombas, Ann. Phys. (Leipzig) 10 (1952) 253.
- [28] C. Titin-Schnaider and P. Quentin, Phys. Lett. B 49 (1974) 397.